

Fluorescence Quenching in Conjugated Polymers Blended with Reduced Graphitic Oxide

Yaobing Wang, Dharmalingam Kurunthu, Gary W. Scott, and Christopher J. Bardeen*

Department of Chemistry, University of California, 501 Big Springs Road, Riverside, California 92521

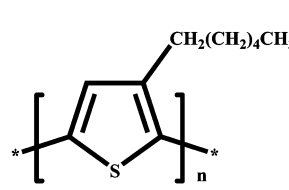
Received: October 12, 2009; Revised Manuscript Received: December 31, 2009

Conjugated polymers blended with graphene represent a possible approach for making organic bulk heterojunction solar cells. In this paper, the time-resolved fluorescence dynamics of poly(3-hexylthiophene-2,5-diyl) (P3HT) and poly[2-methoxy-5-(2'-ethylhexyloxy)-1,4-phenylenevinylene] (MEH-PPV) blended with graphene microsheets derived from chemically reduced graphitic oxide are studied. Both polymers exhibit strong quenching and shortened fluorescence lifetimes when mixed with graphene. The fluorescence quenching function takes the form of $e^{-k_Q t^{1/2}}$, where k_Q is linearly proportional to the weight fraction of graphene in the blend. We consider two physical models to explain the origin of the fluorescence quenching. The first assumes that energy transfer occurs within a three-dimensional space to molecular scale defects within the graphene according to the standard Forster model with an energy transfer rate proportional to the donor–acceptor separation R^{-6} . The second model assumes a quasi-two-dimensional environment where the energy transfer rate between the donor and graphene sheets is proportional to R^{-4} . Using the second model, an estimate of ~ 5 nm is obtained for the critical energy transfer radius for energy transfer between P3HT chains and graphene sheets. This value is in reasonable agreement with theory. Differences between the quenching behavior of graphene in MEH-PPV and P3HT blends are also discussed.

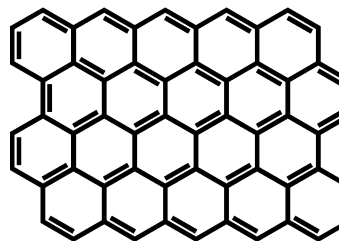
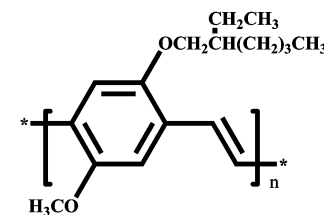
Introduction

Graphene is an allotrope of carbon consisting of a single two-dimensional (2D) layer of sp^2 hybridized carbon atoms. It is currently the subject of intense research interest due to its unique electronic properties.^{1,2} In addition to its very high charge mobilities and coherent quantum transport phenomena, its optical properties are beginning to be studied as well. Recent work has shown that bulk heterojunction layers, consisting of graphene blended with the conjugated polymer P3HT, can function as reasonably efficient organic photovoltaic cells.^{3,4} In these cells, graphene was observed to be a highly effective quencher for the conjugated polymer fluorescence. Graphene and its partially oxidized form graphitic oxide (GO) also been observed to quench the fluorescence of several other organic chromophores in solution, notably pyrene derivatives, and GO has recently been incorporated into organic sensor assemblies that utilize fluorescence quenching to detect biological molecules.^{5–8} The mechanism of the fluorescence quenching in most of these systems has not been extensively characterized. Graphene is a zero energy band gap semiconductor that exhibits metallic behavior in many respects. Like metals, both electronic energy transfer and charge transfer may play a role in fluorescence quenching, depending on the distance of the donor from the metal surface.^{9,10} While the standard Forster resonance energy transfer (FRET) model for two molecules separated by distance R leads to a R^{-6} distance dependence of the electronic energy transfer rate (k_{EET}), the situation can be different when metallic surfaces are involved. Recent theoretical work has suggested that graphene should act as an energy acceptor with its metallic nature and 2D geometry leading to a R^{-4} distance dependence of k_{EET} .^{11,12} While this distance dependence has been observed experimentally for molecules interacting with thin metal films,¹³ it has yet to be confirmed experimentally for graphene.

P3HT



MEH-PPV



Graphene

Figure 1. Molecular structures of the conjugated polymers P3HT and MEH-PPV and of pristine graphene.

Additional experimental work is needed in order to provide insight into the nature of the electronic interactions between graphene and other types of conjugated molecules. A better understanding of such interactions is important if graphene is to become a functional element of organic electronic devices.

Motivated by the observation of photovoltaic activity of graphene/conjugated polymer blend films, we decided to examine the fluorescence quenching of such blends in greater detail. Both poly(3-hexylthiophene-2,5-diyl) (P3HT) and poly[2-methoxy-5-(2'-ethylhexyloxy)-1,4-phenylenevinylene] (MEH-PPV) are polymers commonly used in organic photovoltaic applications, and the chemical structures of all three compounds used in this study are shown in Figure 1. Micrometer-scale graphene sheets are obtained via the chemical reduction of GO, and in this paper these sheets will be referred to as reduced

* To whom correspondence should be addressed, christopher.bardeen@ucr.edu.

graphitic oxide (rGO) to distinguish them from pristine graphene obtained directly from exfoliation of graphite. We find that when the polymers are blended with the rGO, their fluorescence lifetimes decrease in proportion to the amount of added rGO. By experimentally extracting the part of the decay due to the added quencher, as opposed to the intrinsic decay of the neat polymer, we find that the quenching decay can be fit with a stretched exponential of the form $e^{-k_Q t^{1/2}}$. This form of the decay is typically seen in a three-dimensional network of point-dipole quenchers with $k_{EET} \propto R^{-6}$.^{14–17} For the conjugated polymer/rGO blends, we postulate that a more physically accurate picture involves a two-dimensional distribution of quenchers composed of randomly placed graphene walls surrounding the donor with $k_{EET} \propto R^{-4}$, which also leads to the observed $e^{-k_Q t^{1/2}}$ shape of the decay. Thus our quenching data are consistent with the theoretically predicted distance dependence of energy transfer to rGO, although it is not conclusively proven by our data. Quantitative analysis of the quenching constant k_Q is complicated by the lack of precise chemical knowledge about both the donor (presumably an oligomeric segment of the larger polymer chains) and the acceptor (a rGO sheet containing an unknown density of defects). Using reasonable assumptions about the effective density of the rGO sheets, however, permits us to estimate the critical radius $R_0 \sim 5$ nm for energy transfer from P3HT to graphene.

Experimental Section

The graphite powder, 98% anhydrous hydrazine, P3HT, and MEH-PPV from Sigma-Aldrich and P_2O_5 and chloroform from Fisher were all used as received without further purification. Graphite oxide (GO) was synthesized from graphite powder using a modified Hummers method.^{18–20} Fifteen milligrams of the GO film was dispersed directly into a 98% anhydrous hydrazine solution (10 mL) in a nitrogen-filled drybox and allowed to stir for 1 week. The hydrazine solution was then evaporated, and the resulting solid was dried with P_2O_5 . The solid rGO could then be resuspended in a variety of solvents. To make blended films, a chloroform dispersion of fresh rGO was mixed with a chloroform solution of the polymer (P3HT or MEH-PPV) in different ratios, and the resulting mixed solution was then drop cast onto a microscope slide.

The morphologies of the blend film were investigated with a Philips XL30 scanning electron microscope (SEM) equipped with a field emission gun operated at 20 kV. The Raman spectra were collected by a Renishaw H13325 spectrophotometer with laser excitation at 514.5 nm. Absorption spectra of the samples were collected at room temperature with an Ocean Optics S2000 spectrophotometer.

Fluorescence lifetime measurements were carried out using 150 fs pulses centered at 400 nm generated by a 40 kHz regeneratively amplified Ti:sapphire laser system using frequency doubling in a Type I BBO crystal. The 400 nm light was separated from the residual fundamental 800 nm light using a dichroic mirror and two BG39 Schott glass filters. The solid samples were placed in an evacuated cryostat to avoid oxygen quenching. The photoluminescence of the films was collected in front face excitation configuration; i.e., the incident angle of the exciting laser beam was about 10° relative to the film surface normal. The excitation pulses exhibited linear polarization, and the angle between the polarization of the collected fluorescence light and that of the excitation light was adjusted to 54.7° (magic angle), using a thin film polarizer, in order to eliminate time-dependent effects due to molecular reorientation. The fluorescence light was directed into a monochromator attached to a

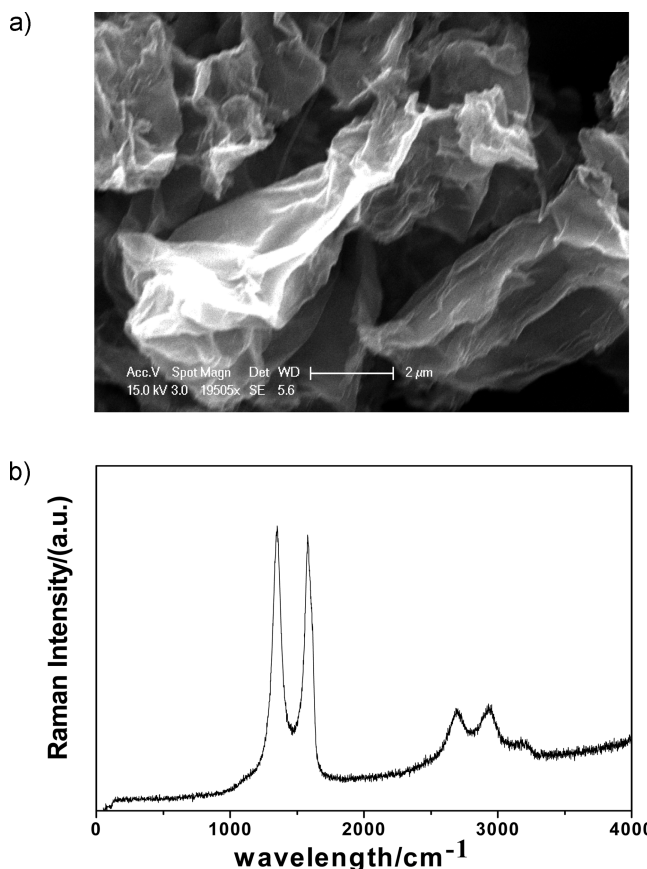


Figure 2. (a) SEM image of rGO microsheets deposited on a glass surface. (b) Raman spectrum of the solid rGO flakes shown in panel a.

picosecond streak camera (Hamamatsu C4334 Streakscope), which provides both time- and wavelength-resolved fluorescence data, with resolutions of 15 ps and 2.5 nm, respectively. Scattered excitation light was removed by placing two GG435 Schott glass filters in front of the streak camera. Varying the excitation pulse energies (35, 75, and 350 pJ) did not change the observed lifetimes, eliminating the possibility of intensity-dependent dynamics. Also the absence of a photobleaching process is confirmed by repeating the experiment in the same position of sample for constant excitation pulse energy.

Results and Discussion

A major challenge in the area of graphene research is the preparation and characterization of the material itself. The graphene studied in this paper is produced chemically by abrasion of graphite, oxidation to GO in order to separate individual sheets, and finally reduction of the GO layers to generate graphene.¹⁹ The graphene generated in this manner usually has inferior transport properties to that produced by exfoliation of graphite²¹ but has the advantage that it is far easier to work with and combine with other molecules. We obtained micrometer-scale sheets of carbon material as shown in Figure 2a. The sheets in these SEM images resemble what has been reported before for rGO prepared in this manner.^{22,23} The presence of rGO in our samples was confirmed by the characteristic peaks of the graphene sp² carbons in the Raman spectrum of this material^{24,25} as shown in Figure 2b. The strong side peak at 1600 cm⁻¹ is indicative of the presence of chemical and geometrical (edge, surface distortions) defects. The relative intensities of the 1350 and 1580 cm⁻¹ peaks indicate that our

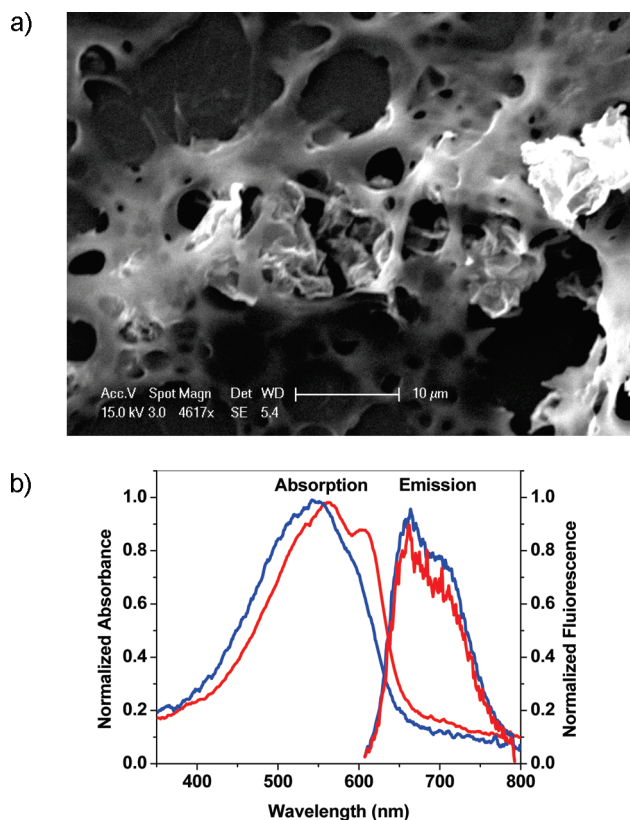


Figure 3. (a) SEM image of P3HT film containing 50% by weight rGO. Note the crumpled rGO sheets below the polymer surface. (b) Absorption and fluorescence spectra of neat P3HT film (blue line) and 50:50 P3HT/graphene film (red line).

rGO is of comparable quality to that used in other experiments measuring thermal and electronic transport properties.^{23,26–31} When a suspension of rGO microsheets in chloroform is mixed with a conjugated polymer solution in the same solvent, it is straightforward to make a homogeneous thin film by spin or drop casting. When the spin-cast films are examined using SEM, as shown in Figure 3a, the crumpled rGO sheets can be seen lying below the film surface, confirming their presence in the polymer. Inspection of the SEM images on larger length scales indicates that the rGO sheets are uniformly distributed within the film. We saw no evidence for aggregation or phase separation on the micrometer length scale. The presence of the rGO microsheets has an observable effect on the absorption spectrum of the polymer film. Figure 3b compares the absorption of a neat P3HT film with that containing 50% rGO by weight. Even at 50% loading, the contribution of the graphene in the visible region of the spectrum is negligible, similar to what has been observed by previous workers.⁴ This is because the absorption coefficients of graphene and rGO^{32–34} are at least 10× smaller than P3HT in this region^{35,36} and also because the graphene absorption spectrum is featureless in this region.^{32,37} At higher concentrations, its main contribution is to enhance the P3HT absorption peak at 610 nm, which is an indicator of the crystallinity of the P3HT. It is possible that the aromatic surface of the graphene regions acts as a template to improve the ordering of the P3HT. This improved ordering is usually achieved by annealing the neat polymer or using other types of chemical additives.^{38–42} But other than this ordering effect, there is no sign of complex formation or new electronic states separate from the absorption spectrum of neat P3HT. The time-integrated fluorescence spectrum of P3HT, with and without the added rGO, is also shown in Figure 3b. There is no discernible change

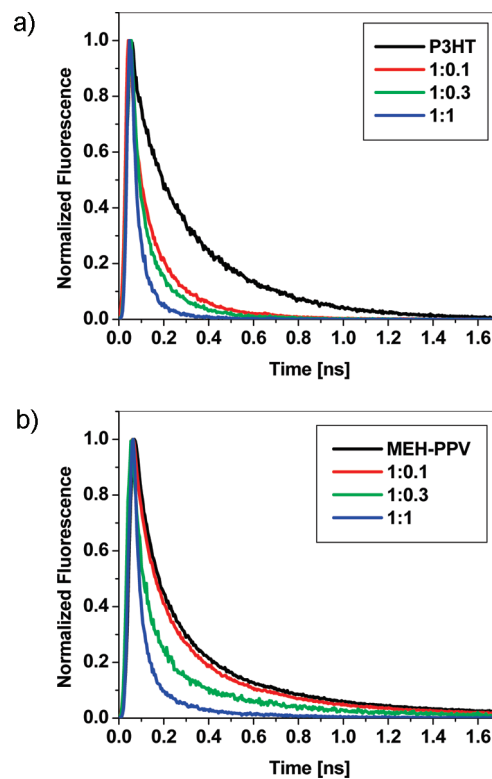


Figure 4. (a) Fluorescence decays of P3HT polymer blended with varying amounts of reduced graphitic oxide: pristine P3HT (black), 1:0.1 P3HT/rGO (red), 1:0.3 P3HT/rGO (green), and 1:1 P3HT/rGO (blue). (b) Fluorescence decays of MEH-PPV polymer blended with varying amounts of reduced graphitic oxide: pristine MEH-PPV (black), 1:0.1 MEH-PPV/rGO (red), 1:0.3 MEH-PPV/rGO (green), and 1:1 MEH-PPV/rGO (blue).

in the spectral shape. To first order, the electronic structures of both rGO and P3HT appear to be unaffected by their proximity to each other.

But while P3HT's electronic states appear to be unaffected by mixing, the relaxation dynamics out of those states are dramatically different. Parts a and b of Figure 4 show the fluorescence decays of P3HT and MEH-PPV, respectively, as the proportion of rGO is increased from 0% to 50% of the total solid by weight. At 0% rGO, the fluorescence decay of P3HT decays to its 1/e value within 250 ps, in reasonable agreement with previous measurements,^{43,44} while MEH-PPV decays with a 1/e time of about 200 ps.^{45,46} In both polymers, the decay becomes roughly a factor of 10 more rapid at the highest rGO loading conditions. The effect of the rGO on the fluorescence decay was somewhat dependent on sample. Samples that had been allowed to sit for >24 h tended to show greater quenching than freshly prepared samples, with k_Q values roughly a factor of 2 greater for the older samples. It appears that packing and the nanostructure of the blended film continue to evolve even after evaporation of the casting solvent. The data in this paper are from samples that have been allowed to age for at least 1 day. For the decays in Figure 4, the fluorescence signal was integrated over the entire spectrum, from 610 to 790 nm. By integrating over a narrower wavelength range, we could examine whether different parts of the spectrum exhibited different decay rates, which would provide evidence of inhomogeneous quenching of different polymer conformations. For both neat P3HT and the blends, no wavelength dependence of the decays was found, indicated that the quenching can be analyzed in terms of a single process. Since both conjugated polymers exhibit nonexponential decays even in their pure form, it is not

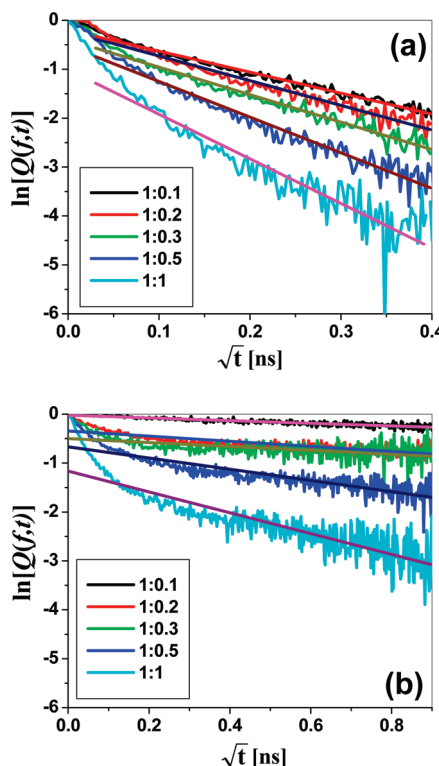


Figure 5. Plot of the quenching function $Q(f,t)$, obtained using eq 1, versus $t^{1/2}$, for (a) P3HT/graphene and (b) MEH-PPV/graphene blend films with different weight:weight ratios.

straightforward to extract a well-defined quenching time by simply fitting the fluorescence decay curves with an accelerated single exponential decay. Instead, we extract the quenching component by dividing the experimentally measured fluorescence decay for a given weight fraction f of rGO, $I(f,t)$ by that of the neat polymer, $I(0,t)$. In this way to obtain a quenching function $Q(f,t)$

$$Q(f,t) = \frac{I(f,t)}{I(f=0,t)} \quad (1)$$

This approach divides out the complex time dependence inherent in the neat polymer decay $I(f=0,t)$ and leaves only the quenching component due to the added rGO. For the remainder of the paper, we will concentrate on the P3HT data, since it is more relevant for solar cell applications and we have more data on that material. Parts a and b of Figure 5 show plots of the $Q(f,t)$ curves obtained from typical P3HT and MEH-PPV samples. These decays cannot be fit well using a single exponential function, but when the log of the signal is plotted versus $t^{1/2}$, we find that the tails of these plots are essentially linear. The advantage of this second representation of the $Q(f,t)$ data is that it illustrates that these functions can be well-described by a function of the form

$$Q(f,t) = \exp[-k_Q(f)t^{1/2}] \quad (2)$$

where $k_Q(f)$ depends on the fraction f of rGO in the sample. Fits using eq 2 are overlaid with the data in Figure 5. Plots of $k_Q(f)$ versus f for both the P3HT and MEH-PPV blends are shown in Figure 6, along with a linear least-squares fits to the data. These fits yield a slope of 5.3 ± 0.6 and a y intercept of 4.0 for P3HT and a slope of 2.2 ± 0.2 with a y intercept of 0.0

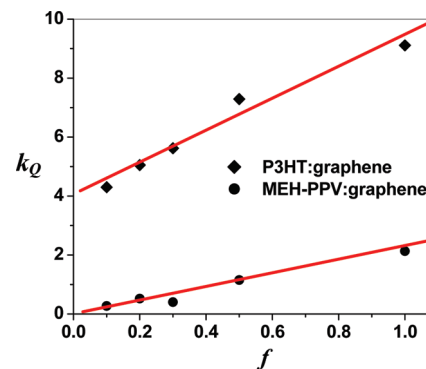


Figure 6. Plot of k_Q versus the fraction of graphene f for the data in Figure 5.

for MEH-PPV. Trying to force the P3HT fit to go through the origin resulted in a much larger error in the slope and a χ^2 error larger by a factor of 20 than that for the nonzero y-intercept fit.

From the data presented above, we conclude that (1) the quenching function $Q(f,t)$ has the stretched exponential form given in eq 2, and (2) $k_Q(f)$ is linearly proportional to f , the fraction of rGO in the blend. The question is then how to explain these observations in the context of the physical properties of the materials. We first consider the case of a donor embedded in a 3D network of acceptors, even though this model may not be a very realistic description of our system. This standard model, used to analyze FRET in many condensed phase systems, is one possible way to produce the $e^{-k_Q t^{1/2}}$ behavior observed in our data. For a 3D system, this temporal behavior results from assuming a Poissonian distribution of acceptors surrounding a single donor, whereupon the decay of the initially excited donor population is given by^{14–17}

$$I_D(t) = \exp\left[\frac{-t}{\tau_D}\right]Q(t) \quad (3a)$$

$$Q(t) = \exp\left[-C_A \int_{DV} (1 - e^{-tw(R)}) C_A(R)\right] \quad (3b)$$

where τ_D is the excited-state lifetime of the donor in the absence of any acceptors, C_A is the density of acceptors, $w(R)$ is the distance-dependent energy transfer rate, and the integration is performed over the entire sample volume. For a three-dimensional system with a uniform distribution of acceptors subject to the standard FRET rate law

$$w(R) = \frac{1}{\tau_D} \left(\frac{R_0}{R}\right)^6 \quad (4)$$

where R_0 is the Forster critical radius, one obtains the well-known result

$$Q(t) = \exp\left[-\frac{4}{3}\pi\Gamma\left(\frac{1}{2}\right)C_A R_0^3 \left(\frac{t}{\tau_D}\right)^{1/2}\right] \quad (5)$$

Equation 5 provides the required $e^{-k_Q t^{1/2}}$ dependence, but its physical interpretation is somewhat muddled in the case where graphene acts as the acceptor. It is difficult to see how micrometer scale sheets of rGO can be approximated as small molecules randomly distributed throughout the three-dimensional material. One possible explanation is that the actual

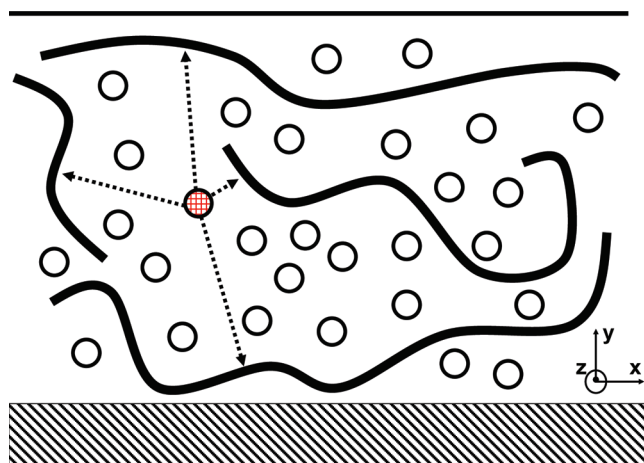


Figure 7. Schematic cross section of a graphene/polymer blend film showing how parallel graphene sheets can create a random two-dimensional array of quenchers around a single excited donor site. Solid lines represent graphene sheets, empty circles are unexcited conjugated polymer segments, and the filled circle represents an excited segment that interacts with surrounding graphene sheets.

quenching does not occur between the donor and the sheet but between the donor and smaller graphene regions within the sheet. The Raman data indicate the presence of defects within the rGO sheets, and it is possible that these defects result in a random assortment of smaller quenching centers within a larger sheet. The presence of discrete quenching “hotspots”, combined with deformation or crumpling of the sheets, may lead to a distribution that looks three-dimensional to individual donor sites. Note that this scenario presupposes that the size of the acceptor defects within the rGO is on the order of a single molecule, so that the FRET requirement of localized dipoles interacting via Coulomb forces is fulfilled.

An alternative mechanism for the quenching takes the 2D nature of the rGO sheets into account. It has been shown experimentally that molecules above a metallic surface undergo energy transfer to the surface with a rate that depends on R^{-3} for a bulk metal or R^{-4} for a thin film, where R is now the distance between the molecule and the surface.^{9,10,13} This type of distance dependence has been predicted for energy donor interacting with graphene.^{11,12} In this case

$$w(R) = \frac{1}{\tau_D} \left(\frac{R_0}{R} \right)^4 \quad (6)$$

Given this rate law, the next question is the spatial extent of the quenching environment. If we imagine parallel sheets of graphene with polymer filling the intervening spaces, from the point of view of an individual donor chromophore, there will be a two-dimensional array of quenchers. This situation is illustrated schematically in Figure 7. The idea is that the parallel sheets form corridors which have random widths in the x and y dimensions, but which prevent the intrusion of sheets along the z dimension. In this way, the third dimension, parallel to the sheets, is prevented from contributing to the quencher distribution by packing constraints. We arrive at an expression for the R^{-4} energy transfer process operating in a two-dimensional space

$$Q(t) = \exp \left[-2\pi C_A \int_0^\infty dr r \left(1 - \exp \left[\frac{-t(R_0)}{\tau_D} \right] \right) \right] \quad (7)$$

After a change of variables and integration by parts, we find

$$Q(t) = \exp \left[-\pi \Gamma \left(\frac{1}{2} \right) C_A R_0^2 \left(\frac{t}{\tau_D} \right)^{1/2} \right] \quad (8)$$

This is a second way to derive the experimentally observed form of $Q(f,t)$ and may be more physically appropriate for our system. The precise determination of which distance dependence holds in the case of graphene, R^{-6} or R^{-4} , will probably require the preparation of well-defined layered systems where the distance between the graphene surface and the donor chromophore can be controlled by chemical methods.⁴⁷ Nevertheless, we can say that our data are consistent with a R^{-4} decay law operating in a quasi-two-dimensional environment.

The next issue concerns whether we can use our data to extract quantitative information about parameters like C_A or R_0 . In the case of three-dimensional FRET-type quenching, it is difficult to extract much useful information, since both the defect concentration C_A and the critical radius R_0 are completely unknown. Obviously C_A would increase linearly with rGO content, but the exact determination of C_A would require knowledge of the defect density within a rGO sheet. Similarly, to estimate R_0 , one would have to have some idea of the detailed chemical structure of the defect. Neither piece of information is available given the current state of knowledge about this novel material. If we instead use the second model that assumes that the fluorescence quenching is due to the sheets arranged in a quasi-two-dimensional space around the donor, we can make a preliminary estimate of R_0 . If we take the average persistence length L of a rGO sheet to be $\sim 1 \mu\text{m}$ as estimated from the SEM image in Figure 2, and its thickness $d = 0.34 \text{ nm}$ as typically estimated for graphene,⁴⁸ we can obtain an estimate for C_A using the physical picture in Figure 7

$$LdC_A = f = \text{fraction of graphene} \quad (9)$$

Note that eq 9 assumes that the graphene sheets are uniformly distributed and do not aggregate. If aggregation played a role, with neighboring sheets clinging together in a face-to-face fashion, the exposed surface area, and thus C_A , would not necessarily scale linearly with f . Nevertheless, eq 9 allows us to obtain a rough estimate of C_A , we can then extract the effective quenching radius R_0 from the slope of our plot of k_Q versus f

$$k_Q = \pi^{3/2} R_0^2 \frac{1}{\sqrt{\tau_D}} C_A = \pi^{3/2} R_0^2 \frac{1}{\sqrt{\tau_D}} \frac{1}{Ld} f \quad (10)$$

Equation 10 predicts the observed linear dependence of k_Q on f , but with a y intercept of 0, not $4.2 \text{ ns}^{-0.5}$ as obtained from the linear least-squares fit of the data in Figure 6. Physically, this suggests that there is an additional quenching mechanism that leads to the offset. This discrepancy is not too surprising in light of the fact that the $e^{-k_Q t^{1/2}}$ dependence was only observed for the tail of the quenching decay. Other types of quenching mechanisms, like charge transfer, may be operative at early times. This definitely seems to be the case for the P3HT data

analyzed here, where even $f = 0.1$ leads to a large amount of quenching as seen in Figure 4a. Nevertheless, while keeping in mind its limitations, it is instructive to analyze the P3HT data in Figure 6 using eq 10. If we take $\tau_D = 250$ ps to be the 1/e time for the fluorescence decay of neat P3HT, we find $R_0 \sim 5$ nm. This value is comparable to that predicted theoretically, although given the crude nature of this model, the agreement may be more fortuitous than definitive. Nevertheless, we can show that for reasonable assumptions about geometry of the rGO sheets embedded in the polymer film, our model at least gives reasonable values for R_0 .

Finally, it is instructive to briefly compare the P3HT dynamics with those of the MEH-PPV blends. This comparison will be made within the context of the 2D quenching model described in the preceding paragraph, despite the fact that this model is not conclusively established. First, we note that the qualitative behavior of the fluorescence quenching is similar for both polymers: both exhibit the $e^{-k_Q f^{1/2}}$ behavior and in both cases k_Q scales linearly with f , as shown in Figure 6. The first important difference between the two data sets is that MEH-PPV appears to have a weaker dependence on the rGO fraction f . Since the fluorescence lifetimes (τ_D) are similar for the two polymers, this suggests that the R_0 value is slightly smaller for MEH-PPV. A second noticeable difference is that the linear fit to the MEH-PPV data in Figure 6 passes through the origin, unlike P3HT. Thus it appears that the energy transfer mechanism by itself is sufficient to describe the fluorescence quenching in this blend, without recourse to a second, more rapid mechanism as appears to be the case in P3HT. This is consistent with the observation that the MEH-PPV data in Figure 4b does not have the same sensitivity as P3HT to low concentrations of rGO. Thus a comparison of the MEH-PPV and P3HT data suggests that the fluorescence quenching dynamics of rGO is sensitive to the chemical structure of the donor polymer, as would be expected for molecular-level processes like energy or charge transfer.

Conclusion

The data in this paper show that microsheets of graphene are effective fluorescence quenchers for the conjugated polymers P3HT and MEH-PPV. We find the temporal behavior of the quenching function to be of the form $e^{-k_Q f^{1/2}}$ where k_Q depends linearly on the amount of rGO in the blended film. In order to explain the time dependence of the quenching, we consider two distinct physical mechanisms. The first assumes that the quenching is dominated by FRET to molecular-like defects that are randomly distributed in three dimensions by the folding and rippling of the sheets. An alternate mechanism relies on the intact sheets giving rise to a quasi-two-dimensional environment where the energy donors are trapped in long corridors between randomly spaced sheets. When the theoretically predicted R^{-4} distance dependent quenching for graphene is assumed, this model also results in the observed time dependence. A full understanding of how energy transfer and fluorescence quenching occurs in graphene will probably have to wait until very well defined layered structures can be developed, in analogy with earlier work on molecular fluorescence quenching near metal surfaces.⁴⁷ But the present work demonstrates not only that graphene sheets are effective fluorescence quenching agents but also that their mechanism is at least consistent with that of a lower dimensional, R^{-4} metallic type of quenching.

Acknowledgment. C.J.B. acknowledges the support of the National Science Foundation, Grant CHE-0719039.

References and Notes

- (1) Geim, A. K. Graphene: status and prospects. *Science* **2009**, *324*, 1530–1534.
- (2) Neto, A. H. C.; Geinea, F.; Peres, N. M. R.; Novoselov, K. S.; Geim, A. K. The electronic properties of graphene. *Rev. Mod. Phys.* **2009**, *81*, 109–162.
- (3) Liu, Z.; Liu, Q.; Huang, Y.; Ma, Y.; Yin, S.; Zhang, X.; Sun, W.; Chen, Y. Organic photovoltaic devices based on a novel acceptor material: graphene. *Adv. Mater.* **2008**, *20*, 3924–3930.
- (4) Liu, Q.; Liu, Z.; Zhang, X.; Yang, L.; Zhang, N.; Pan, G.; Yin, S.; Chen, Y.; Wei, J. Polymer photovoltaic cells based on solution-processable graphene and P3HT. *Adv. Funct. Mater.* **2009**, *19*, 894–904.
- (5) Xu, Y.; Bai, H.; Li, C.; Shi, G. Flexible graphene films via the filtration of water-soluble noncovalent functionalized graphene sheets. *J. Am. Chem. Soc.* **2008**, *130*, 5856–5857.
- (6) Yang, X.; Zhang, X.; Liu, Z.; Ma, Y.; Huang, Y.; Chen, Y. High-efficiency loading and controlled release of doxorubicin hydrochloride on graphene oxide. *J. Phys. Chem. C* **2008**, *112*, 17554–17558.
- (7) Liang, Y.; Wu, D.; Feng, X.; Mullen, K. Dispersion of graphene sheets in organic solvent supported by ionic interactions. *Adv. Mater.* **2009**, *21*, 1679–1683.
- (8) Lu, C.-H.; Yang, H.-H.; Zhu, C.-L.; Chen, X.; Chen, G.-N. A graphene platform for sensing biomolecules. *Angew. Chem., Int. Ed.* **2009**, *48*, 4785–4787.
- (9) Chance, R. R.; Prock, A.; Silbey, R. Molecular fluorescence and energy transfer near interfaces. *Adv. Chem. Phys.* **1978**, *37*, 1–65.
- (10) Persson, B. N. J.; Lang, N. D. Electron-hole-pair quenching of excited states near a metal. *Phys. Rev. B* **1982**, *26*, 5409–5414.
- (11) Swathi, R. S.; Sebastian, K. L. Resonance energy transfer from a dye molecule to graphene. *J. Chem. Phys.* **2008**, *129*, 054703/1–054703/9.
- (12) Swathi, R. S.; Sebastian, K. L. Long range resonance energy transfer from a dye molecule to graphene has $(\text{distance})^{-4}$ dependence. *J. Chem. Phys.* **2009**, *130*, 086101/1–086101/3.
- (13) Alivisatos, A. P.; Waldeck, D. H.; Harris, C. B. Nonclassical behavior of energy transfer from molecules to metal surfaces: Biacetyl(3np*)/Ag(111). *J. Chem. Phys.* **1985**, *82*, 541–547.
- (14) Yekta, A.; Duhamel, J.; Winnik, M. A. Dipole-dipole electronic energy transfer. Fluorescence decay functions for arbitrary distributions of donors and acceptors: systems with planar geometry. *Chem. Phys. Lett.* **1995**, *235*, 119–125.
- (15) Baumann, J.; Fayer, M. D. Excitation transfer in disordered two-dimensional and anisotropic three-dimensional systems: effects of spatial geometry on time-resolved observables. *J. Chem. Phys.* **1986**, *85*, 4087–4107.
- (16) Blumen, A. Excitation transfer from a donor to acceptors in condensed media: a unified approach. *Nuovo Cimento* **1981**, *63 B*, 50–58.
- (17) Drake, J. M.; Klafter, J.; Levitz, P. Chemical and biological microstructures as probed by dynamic processes. *Science* **1991**, *251*, 1574–1579.
- (18) Hummers, W. S.; Offeman, R. E. Preparation of graphitic oxide. *J. Am. Chem. Soc.* **1958**, *80*, 1339.
- (19) Tung, V. C.; Allen, M. J.; Yang, Y.; Kaner, R. B. High-throughput solution processing of large-scale graphene. *Nat. Nanotechnol.* **2008**, *4*, 25–29.
- (20) Park, S.; Ruoff, R. S. Chemical methods for the production of graphenes. *Nat. Nanotechnol.* **2009**, *4*, 217–224.
- (21) Eda, G.; Mattevi, C.; Yamaguchi, H.; Kim, H.; Chhowalla, M. Insulator to semimetal transition in graphene oxide. *J. Phys. Chem. C* **2009**, *113*, 15768–15771.
- (22) Hirata, M.; Gotou, T.; Horiuchi, S.; Fujiwara, M.; Ohba, M. Thin-film particles of graphite oxide 1: High-yield synthesis and flexibility of the particles. *Carbon* **2004**, *42*, 2929–2937.
- (23) Tang, L.; Wang, Y.; Li, Y.; Feng, H.; Lu, J.; Li, J. Preparation, structure, and electrochemical properties of reduced graphene sheet films. *Adv. Funct. Mater.* **2009**, *19*, 2782–2789.
- (24) Ferrari, A. C.; Meyer, J. C.; Scardaci, V.; Casiraghi, C.; Lazzeri, M.; Mauri, F.; Piscanec, S.; Jiang, D.; Novoselov, K. S.; Roth, S.; Geim, A. K. Raman spectrum of graphene and graphene layers. *Phys. Rev. Lett.* **2006**, *97*, 187401/1–187401/4.
- (25) Malard, L. M.; Pimenta, M. A.; Dresselhaus, G.; Dresselhaus, M. S. Raman spectroscopy in graphene. *Phys. Rep.* **2009**, *473*, 51–87.
- (26) Gomez-Navarro, C.; Weitz, R. T.; Bittner, A. M.; Scolari, M.; Mews, A.; Burghard, M.; Kern, K. Electronic transport properties of individual chemically reduced graphene oxide sheets. *Nano Lett.* **2007**, *7*, 3499–3503.
- (27) Lv, X.; Huang, Y.; Liu, Z.; Tian, J.; Wang, Y.; Ma, Y.; Liang, J.; Fu, S.; Wan, X.; Chen, Y. Photoconductivity of bulk-film-based graphene sheets. *Small* **2009**, *5*, 1682–1687.
- (28) Pan, D.; Wang, S.; Zhao, B.; Wu, M.; Zhang, H.; Wang, Y.; Jiao, Z. Li storage properties of disordered graphene sheets. *Chem. Mater.* **2009**, *21*, 3136–3142.

- (29) Lee, V.; Whittaker, L.; Jaye, C.; Baroudi, K. M.; Fischer, D. A.; Banerjee, S. Large-area chemically modified graphene films: electrophoretic deposition and characterization by soft x-ray absorption spectroscopy. *Chem. Mater.* **2009**, *21*, 3905–3916.
- (30) Zhou, Y.; Bao, Q.; Tang, L. A. L.; Zhong, Y.; Loh, K. P. Hydrothermal dehydration for the “green” reduction of exfoliated graphene oxide to graphene and demonstration of tunable optical limiting properties. *Chem. Mater.* **2009**, *21*, 2950–2956.
- (31) Sreeprasad, T. S.; Samal, A. K.; Pradeep, T. Tellurium nanowire-induced room temperature conversion of graphite oxide to leaf-like graphenic structures. *J. Phys. Chem. C* **2009**, *113*, 1727–1737.
- (32) Niyogi, S.; Bekyarova, E.; Itkis, M. E.; McWilliams, J. L.; Harmon, M. A.; Haddon, R. C. Solution properties of graphite and graphene. *J. Am. Chem. Soc.* **2006**, *128*, 7720–7721.
- (33) Hernandez, Y.; Nicolosi, V.; Lotya, M.; Blighe, F. M.; Sun, Z.; De, S.; McGovern, I. T.; Holland, B.; Byrne, M.; Gunko, Y. K.; Boland, J. J.; Niraj, P.; Duesberg, G.; Krishnamurthy, S.; Goodhue, R.; Hutchison, H.; Scardaci, V.; Ferrari, A. C.; Coleman, J. N. High-yield production of graphene by liquid-phase exfoliation of graphite. *Nat. Nanotechnol.* **2008**, *3*, 563–568.
- (34) Hamilton, C. E.; Lameda, J. R.; Sun, Z.; Tour, J. M.; Barron, A. R. High-yield organic dispersions of unfunctionalized graphene. *Nano Lett.* **2009**, *9*, 3460–3462.
- (35) Choulis, S. A.; Kim, Y.; Nelson, J.; Bradley, D. D. C.; Giles, M.; Shkunov, M.; McCulloch, I. High ambipolar and balanced carrier mobility in regioregular poly(3-hexylthiophene). *Appl. Phys. Lett.* **2004**, *85*, 3890–3892.
- (36) Scully, S. R.; McGehee, M. D. In *Flexible Electronics*; Wong, W. S., Salleo, A., Eds.; Springer: New York, 2009.
- (37) Li, D.; Muller, M. B.; Gilje, S.; Kaner, R. B.; Wallace, G. G. Processable aqueous dispersions of graphene nanosheets. *Nat. Nanotechnol.* **2008**, *3*, 101–105.
- (38) Padinger, F.; Rittberger, R. S.; Sariciftci, N. S. Effects of postproduction treatment on plastic solar cells. *Adv. Funct. Mater.* **2003**, *13*, 85–88.
- (39) Li, G.; Shrotriya, V.; Huang, J.; Yao, Y.; Moriarty, T.; Emery, K.; Yang, Y. High-efficiency solution processable polymer photovoltaic cells by self-organization of polymer blends. *Nat. Mater.* **2005**, *4*, 864–868.
- (40) Peet, J.; Soci, C.; Coffin, R. C.; Nguyen, T. Q.; Mikhailovsky, A.; Moses, D.; Bazan, G. C. Method for increasing the photoconductive response in conjugated polymer/fullerene composites. *Appl. Phys. Lett.* **2006**, *89*, 252105/1–252105/3.
- (41) Lee, J. K.; Ma, W. L.; Brabec, C. J.; Yuen, J.; Moon, J. S.; Kim, J. Y.; Lee, K.; Bazan, G. C.; Heeger, A. J. Processing additives for improved efficiency from bulk heterojunction solar cells. *J. Am. Chem. Soc.* **2008**, *130*, 3619–3623.
- (42) Bechara, R.; Leclerc, N.; Leveque, P.; Richard, F.; Heiser, T.; Hadzioannou, G. Efficiency enhancement of polymer photovoltaic devices using thieno-thiophene based copolymers as nucleating agents for poly-thiophene crystallization. *Appl. Phys. Lett.* **2008**, *93*, 013306/1–013306/3.
- (43) Clark, J.; Silva, C.; Friend, R. H.; Spano, F. C. Role of intermolecular coupling in the photophysics of disordered organic semiconductors: aggregate emission in regioregular polythiophene. *Phys. Rev. Lett.* **2007**, *98*, 206406/1–206406/4.
- (44) Cook, S.; Furube, A.; Katoh, R. Analysis of the excited states of regioregular polythiophene P3HT. *Energy Environ. Sci.* **2008**, *1*, 294–299.
- (45) Smilowitz, L.; Hays, A.; Heeger, A. J.; Wang, G.; Bowers, J. E. Time-resolved photoluminescence from poly[2-methoxy,5-(2'-ethyl-hexyloxy)-p-phenylenevinylene]: solutions, gels, films and blends. *J. Chem. Phys.* **1993**, *98*, 6504–6509.
- (46) Samuel, I. D. W.; Crystall, B.; Rumbles, G.; Burn, P. L.; Holmes, A. B.; Friend, R. H. The efficiency and time-dependence of luminescence from poly(-phenylene vinylene) and derivatives. *Chem. Phys. Lett.* **1993**, *213*, 472–478.
- (47) Drexhage, K. H. In *Progress in Optics XII*; Wolf, E., Ed.; North-Holland: Amsterdam, 1974; pp 165–232.
- (48) Huang, Y.; Wu, J.; Hwang, K. C. Thickness of graphene and single-wall carbon nanotubes. *Phys. Rev. B* **2006**, *74*, 245413/1–245413/9.

JP9097793